Electronic band structure of zirconia and hafnia polymorphs from the *GW* perspective

Hong Jiang,[1,*] Ricardo I. Gomez-Abal,[1] Patrick Rinke,[1,2] and Matthias Scheffler[1,2]
[1]*Fritz-Haber-Institut der Max-Planck-Gesellschaft, Berlin, Germany*
[2]*University of California at Santa Barbara, Santa Barbara, California 93106, USA*
(Received 13 January 2010; published 24 February 2010)

The electronic structure of crystalline ZrO_2 and HfO_2 in the cubic, tetragonal, and monoclinic phase has been investigated using many-body perturbation theory in the *GW* approach based on density-functional theory calculations in the local-density approximation (LDA). ZrO_2 and HfO_2 are found to have very similar quasiparticle band structures. Small differences between them are already well described at the LDA level indicating that the filled *f* shell in HfO_2 has no significant effect on the *GW* corrections. A comparison with direct and inverse photoemission data shows that the *GW* density of states agrees very well with experiment. A systematic investigation into the structural and morphological dependence of the electronic structure reveals that the internal displacement of the oxygen atoms in the tetragonal phase has a significant effect on the band gap.

DOI: 10.1103/PhysRevB.81.085119 PACS number(s): 71.10.−w, 71.15.−m, 71.20.−b, 71.27.+a

I. INTRODUCTION

Silicon-based microelectronic technology has undergone a paradigm shift at the beginning of this century replacing silicon dioxide (with a dielectric constant of $\kappa=3.9$) by a gate material with a higher κ.[1,2] Until recently the gate material of choice has been silicon's native oxide (SiO_2) and its nitride derivatives. The continual scaling of silica-based field-effect transistors has reduced the gate to ultrathin SiO_2 layers of $\sim$1 nm thickness that exhibit excessive gate leakage currents resulting in intolerably high power dissipation and device breakdown. One of the most prominent solutions to this problem is the use of high-κ materials to achieve physically thicker but capacitively equivalent gate dielectrics.[1] Hafnia (HfO_2) and zirconia (ZrO_2) are currently among the most intensively studied high-κ materials. Both compounds combine a high dielectric constant of $\kappa \approx 6 \times \kappa_{SiO_2}$, with a large band gap, and, more importantly, high potential barriers to silicon for both holes and electrons. In a wider context, hafnia and zirconia are also frequently used in heterogeneous catalysis, as oxygen sensors and in solid oxide fuel cells. Yttria-stabilized zirconia is currently a prominent thermal barrier coating material in gas turbines for power generators and jet engines.[3] Despite their importance, however, a comprehensive first-principles understanding of their electronic structure—although essential for many device considerations—is still lacking.[4–10]

Zirconium (Zr) and Hafnium (Hf) belong to the same group in the periodic table and their main difference in terms of the electronic structure is the *f* states. Hf has a closed 4*f* subshell, whereas Zr has no *f* electrons. As a result of the "poor shielding" provided by the 4*f* electrons the atomic and ionic radii of Hf, although much heavier than Zr, are almost identical to those of Zr. Because of this "lanthanide contraction," Zr and Hf are often regarded as the two chemically most similar homogenesis elements.[11] They do, however, differ in some minor but possibly significant aspects of their chemical and physical properties. At the atomic level, Hf has a slightly smaller electronegativity than Zr (1.16 vs 1.32 in terms of the spectroscopic electronegativity),[12] indicating a slightly stronger tendency to form ionic bonds with other more electronegative elements such as O. This small difference seems to affect the thermodynamic stability of zirconia and hafnia in contact with Si. A combined experimental and theoretical study[13] found that HfO_2 is more stable than ZrO_2 by 42 kJ/mol in the heat of formation, conversely hafnium silicides are less stable than zirconium silicides by $\sim$25 kJ/mol. As a result, the HfO_2/Si interface is stable with respect to silicide formation, but the ZrO_2/Si interface is not, which makes HfO_2 more suitable as a gate dielectric material.

Zirconia and hafnia can exist in several different polymorphic phases, depending on the growth conditions.[14] In thin films zirconia and hafnia are typically amorphous in their as-deposited state[15–18] but nanocrystallites form during high-temperature annealing (typically at $\sim$1000 K). The films preferentially crystallize in the most stable monoclinic structure but the presence of the tetragonal phase and other polymorphs is frequently observed as well.[16,17,19] Different growth techniques (mostly physical-vapor deposition, chemical-vapor deposition, and atomic-layer deposition) (Ref. 2) and different growth conditions produce films of varying quality with different phase compositions, which in turn influences their chemical and physical properties, including, in particular, properties that derive from the electronic structure.[2] As a result, the experimental band gaps of ZrO_2 and HfO_2 are highly scattered (in the range 5–6 eV).[16–29] Recent density-functional theory (DFT) calculations employing screened exchange[30] or hybrid functionals,[9,10] which partially correct the band-gap problem of more conventional DFT calculations, give band gaps in this range, too, but their dependence on adjustable parameters does not permit a unanimous identification. However, a precise determination of the band gap is not only important from a fundamental materials science point of view but also necessary for device design in microelectronics.[1,6,8–10,31]

In this work we report a first-principles study of the electronic band structure of ZrO_2 and HfO_2. We apply many-body perturbation theory in the *GW* approximation,[32] which is currently regarded as the most suitable first-principles approach for the description of the electronic band structure of *sp*-bonded systems.[33–35] Applications to high-κ materials are not as frequent but are also slowly emerging.[4,5,36,37] From the

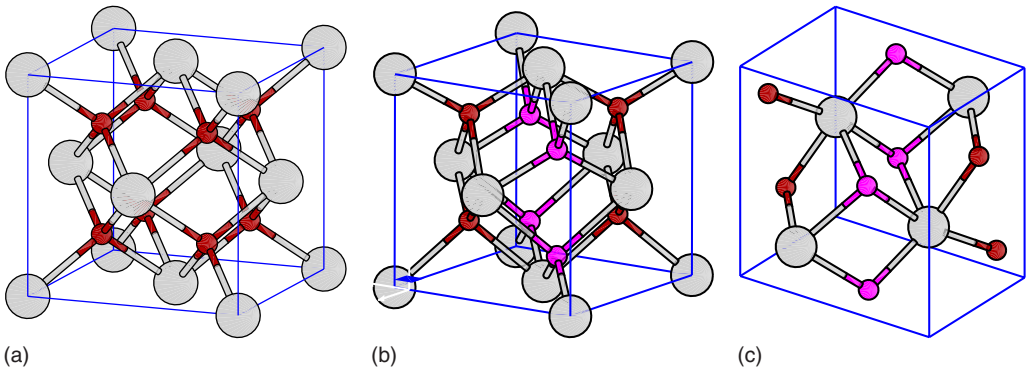

FIG. 1. (Color online) Illustrations of cubic (left), tetragonal (central), and monoclinic (right) lattice structures. Large spheres represent M(=Zr,Hf) atoms and small ones oxygen sites. Red (black) and pink (gray) colors distinguish oxygen atoms that are upward and downward displaced in the tetragonal structure, and the two nonequivalent oxygen atoms in the monoclinic structure.

conceptual point of view, zirconia and hafnia are different from conventional *sp* semiconductors in the sense that the conduction bands (CBs) of these compounds are mainly of *d* character, for which the suitability of the *GW* approximation has not been fully established yet. For *sp* systems with shallow semicore *d* states [e.g., IIB-VI semiconductors (most notably ZnO) or group-III nitrides] *GW* calculations are already more challenging.[35,38–40] Zirconia and hafnia—being the simplest transition-metal oxides—fall between normal (weakly correlated) *sp* systems and highly complex (strongly correlated) *d*- and *f*-electrons systems. A thorough understanding of these materials will therefore be important for first-principles studies of strongly correlated systems, for which an assessment of the *GW* approach is also beginning to emerge.[41–46]

The paper is organized as follows. In Sec. II we briefly describe the theoretical framework and computational approach employed in this work. In Sec. III we present the electronic band structure of ZrO_2 and HfO_2 in different polymorphic phases and compare our theoretical studies with recent experiments. Section IV summarizes the main findings of this work.

II. COMPUTATIONAL METHOD

The state-of-the-art first-principles approach to quasiparticle band structures of real materials as probed by direct and inverse photoemission is many-body perturbation theory in the *GW* approximation.[32,33,47–50] The self-energy in many-body perturbation theory that links the noninteracting with the interacting system is given by the product of the Green's function G and the screened Coulomb interaction W in the random-phase approximation (RPA). In practice the *GW* method is usually applied as a correction to Kohn-Sham (KS) density-functional theory, henceforth denoted G_0W_0. Further improvement can sometimes be gained by including partial self-consistency in the calculation of G with fixed RPA screening (W_0) (see, e.g., Ref. 51), henceforth denoted GW_0. In this work we use both G_0W_0 and GW_0 based on the KS single-particle Hamiltonian in the local-density approximation (LDA) and demonstrate that the GW_0 results are in general in better agreement with available experimental data.

All DFT calculations are performed using the WIEN2K package[52] in which the Kohn-Sham equations are solved in the full-potential (linearized) augmented plane wave plus local-orbital [FP-(L)APW+lo] approach.[53] *GW* calculations were performed using a recently developed all-electron *GW* code.[46,54] Further details of the implementation will be presented elsewhere.[55,56]

Recently we have proposed to use the LDA with a local Hubbard-type correction (LDA+U) as the starting point for *GW* calculations to overcome some of the pathologies of *GW*@LDA for *d*- or *f*-electron systems.[46] In this work we still apply the *GW*@LDA approach for the following reasons: First, the LDA description of the materials considered here is still qualitatively correct and we expect the LDA single-particle Hamiltonian to be a suitable reference for G_0W_0 and GW_0 calculations; second, it has been shown that *GW*@LDA+U results depend only very weakly on U for systems with empty or full d/f shells,[46,57] and *GW*@LDA+U will therefore give essentially the same results as *GW*@LDA.

The dielectric permittivity tensor of zirconia and hafnia is dominated by the ionic or static contribution ϵ_0.[14,58,59] The electronic contribution (ϵ_∞) is a factor 5–6 smaller than ϵ_0.[14,58,59] This is an indication for strong electron-phonon coupling in these materials, which should, in principle, be included in the dielectric function used in the *GW* calculations. However, at present no *GW* calculation that takes electron-phonon coupling into account has been reported and it is not entirely clear how to include the electron-phonon interaction consistently into the formalism.[60–62] For this reason we stick to the state of the art in *GW* and compute the screened Coulomb interaction with only the electronic dielectric function. We expect the band-gap renormalization due to electron-phonon coupling to be on the order of 0.1 eV or less,[63,64] which is smaller than the current experimental resolution for zirconia and hafnia.

Densities of states (DOS) are calculated using ~1000 **k** points in the Brillouin zone. A Gaussian broadening of 0.6 eV was chosen to mimic the typical instrumental resolution in the photoemission spectroscopy/inverse photoemission spectroscopy (PES/IPS) data. For *GW* DOS data, *GW* quasiparticle energies calculated on a sparse **k** mesh[56] are interpolated to the fine **k** mesh (~1000) using the Fourier interpolation technique developed in Ref. 65.

TABLE I. Experimental structural parameters for the different polymorphs of ZrO_2 and HfO_2 used in this work (Ref. 14). Lattice constants a, b, and c are given in Å. In the tetragonal phase, the displacement of the oxygen atom (in units of c) with respect to the position in the ideal cubic phase is denoted as d_z. The coordinates of the M (Zr or Hf) and the two nonequivalent oxygen atoms in the monoclinic phase ($\mathbf{r}_M$ and $\mathbf{r}_{O1}$, $\mathbf{r}_{O2}$) are given as internal coordinates. The experimental value of d_z for t-HfO_2 is not available and due to the similarity between ZrO_2 and HfO_2 is set to that of t-ZrO_2 (for comparison, the optimized value by LDA is d_z=0.061).

Structure		M=Zr	M=Hf
Cubic	a	5.09	5.08
Tetra	a	5.05	5.15
	c	5.18	5.29
	d_z	0.057	0.057
Mono	a	5.15	5.117
	b	5.21	5.175
	c	5.32	5.291
	β	99.23	99.22
	$\mathbf{r}_M$	(0.275,0.040,0.208)	(0.276,0.040,0.208)
	$\mathbf{r}_{O1}$	(0.070,0.332,0.345)	(0.074,0.332,0.347)
	$\mathbf{r}_{O2}$	(0.450,0.756,0.479)	(0.449,0.758,0.480)

III. RESULTS AND DISCUSSIONS

A. Structural parameters

In this work, we consider the three low-pressure phases of MO_2 (M=Zr and Hf): cubic, tetragonal, and monoclinic, as illustrated in Fig. 1. In the simplest structure, the cubic one (c-MO_2, space group $Fm\bar{3}m$), M atoms form a face-centered cubic lattice and oxygen atoms occupy all tetrahedral sites, with one MO_2 formula unit in the primitive unit cell. The tetragonal structure (t-MO_2, space group $P4_2/nmc$) can be obtained by deforming the cubic unit cell along one direction ($c/a>1$) and displacing alternate oxygen atoms in the direction along the tetragonal axis upward and downward with a relative distortion of d_z. The monoclinic structure (m-MO_2, space group $P2_1/c$, also called the baddeleyite structure) has four MO_2 units in the primitive cell with a total of 13 structural parameters; all four M sites are equivalent and sevenfold coordinated, and two nonequivalent oxygen sites are threefold and fourfold coordinated, respectively. The crystalline cubic and tetragonal structures are stable only at high temperature but can be stabilized by the presence of other lower valence metal oxides such as Y_2O_3, CaO, or MgO.[66] In addition, the tetragonal structure has been observed in nanoparticles or ultrathin films.[67] Since the main focus of this work is on the electronic properties of zirconia and hafnia, we use structural parameters from experiment taken from Ref. 14. They are listed in Table I.

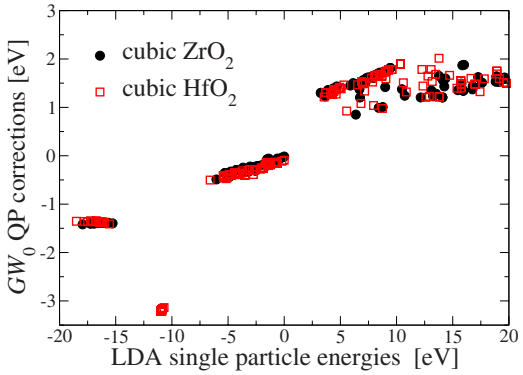

FIG. 3. (Color online) GW_0 quasiparticle corrections of cubic ZrO_2 and HfO_2 as a function of the corresponding LDA eigenvalue.

B. Density of states

We first consider the DOS of different polymorphs of ZrO_2 and HfO_2 obtained in LDA, G_0W_0 and GW_0, as shown in Fig. 2. The most striking feature is the similarity between ZrO_2 and HfO_2 both in LDA and GW. The notable exception is the presence of the semicore f states in HfO_2 between the O $2p$ and O $2s$ bands. This similarity in the DOSs indicates that the filled f shell has no appreciable affect on the upper valence band (VB) of HfO_2. This is also evident from the nearly identical quasiparticle corrections in zirconia and hafnia shown in Fig. 3.

Nevertheless there are several small but significant differences: (1) the band gaps in HfO_2 are slightly larger than those in ZrO_2 (by about 0.3 eV); (2) the VB width of HfO_2 is

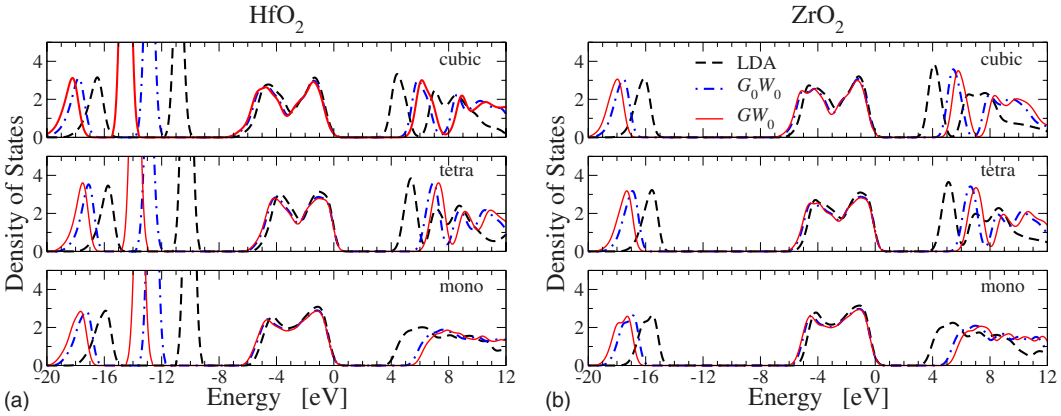

FIG. 2. (Color online) LDA and GW_0 density of states of HfO_2 (left) and ZrO_2 (right) for the cubic, tetragonal, and monoclinic phase.

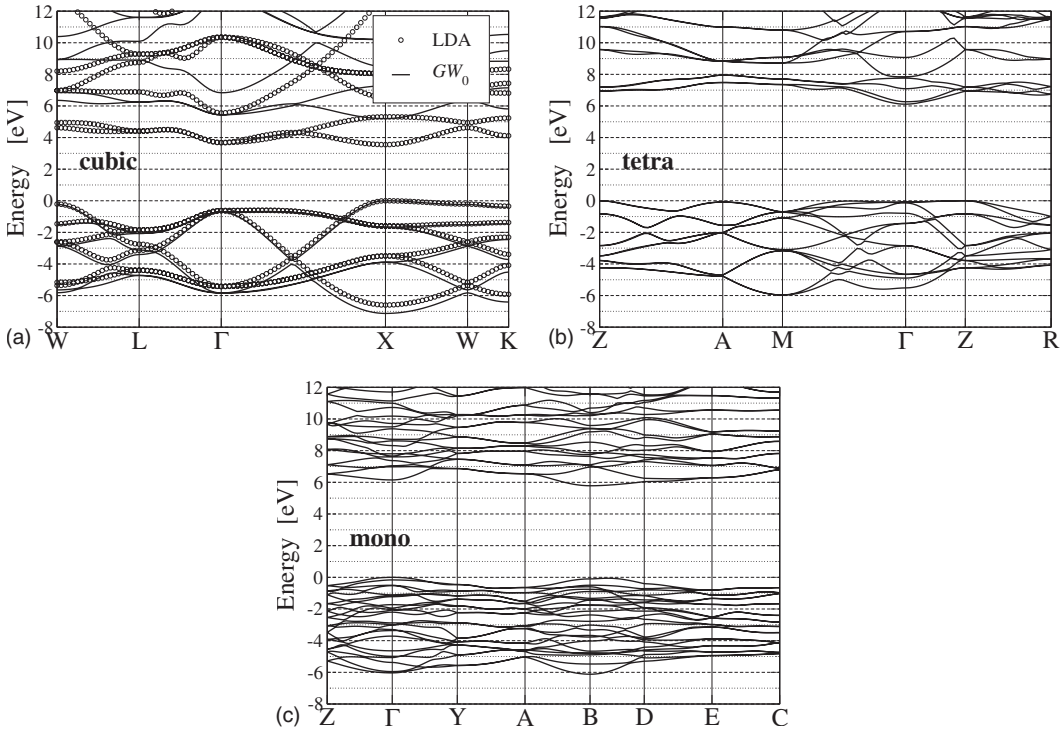

FIG. 4. GW_0 band structures of HfO_2 in the cubic (upper), tetragonal (middle), and monoclinic (lower) phase calculated at the experimental lattice parameters given in Table I. The VBM is taken as energy zero. The nomenclature of the high-symmetry points is taken from Fig. 8 of Ref. 70. For clarity, the LDA band structure is only shown for the cubic phase since the GW_0 corrections mostly shift the valence with respect to the conduction bands and do not change the essential features of the band structure.

approximately 0.6 eV larger than that of ZrO_2; and (3) the crystal-field splitting in the CB is slightly stronger in HfO_2 than in ZrO_2. In addition, c-HfO_2 has a direct minimal gap at the X point, whereas c-ZrO_2 has an indirect gap with the VB maximum (VBM) at X and the CB minimum (CBM) at Γ. These differences are consistent with the known chemistry of Hf and Zr: the electronegativity of Hf is slightly smaller than in Zr and therefore HfO_2 is more ionic and exhibits stronger crystal-field effects than ZrO_2.[68,69] All these differences, however, are present already at the LDA level; the *GW* corrections (cf. Fig. 3) are nearly identical in ZrO_2 and HfO_2, as mentioned above.

Comparing LDA and G_0W_0, we note that the main effects of the G_0W_0 corrections are (1) a significant increase in the band gap by ~1.4 eV, (2) a slight increase in the valence bandwidth, and (3) a significant downward shift of the O 2*s* states by ~1.5 eV and for HfO_2 a downwards shift of the Hf 4*f* states by ~2.5 eV. The GW_0 results are in general quite similar to those of G_0W_0 except that the 4*f* states in HfO_2 are further pushed toward lower energy by ~1.0 eV. The O 2*s* binding energy and the band gaps also increase slightly. The fact that partial self-consistency (GW_0) increases the 4*f* binding energy by ~1 eV is consistent with a previous study by Shishkin and Kresse,[51] who observed a similar amount of increase for 3*d* semicore binding energies of IIB-VI and III-V semiconductors. In the remaining part of the paper we will therefore focus mainly on the GW_0 results since the G_0W_0 results can be easily inferred from those of GW_0 due to their similarity.

With respect to different polymorphs we again observe a remarkable spectral resemblance. The upper valence band looks almost identical in all three phases, but the O 2*s* and Hf 4*f* states lie lower in energy in the cubic phase, compared to the tetragonal and monoclinic one. Moreover, the two pronounced peaks in the conduction band of the cubic and the tetragonal phase are washed out in the monoclinic phase as a result of its lower symmetry.

C. Band structures and band gaps

More detailed information on the electronic structure can be obtained from the band structure. Considering the similarity between ZrO_2 and HfO_2, we only show the band structure of the three different phases of HfO_2 in Fig. 4. The GW_0 corrections to the LDA band structure are essentially *k* independent but energy dependent. This is reflected in the near linear behavior of the quasiparticle corrections shown in Fig. 3, which is typical for *sp*-bonded semiconductors.[48,50,71] In other words, the further a state from the VBM, the larger the GW_0 correction.

The cubic phase has a direct gap at X [$\mathbf{k}=(1,0,0)$] that is nearly degenerate in energy with the indirect X to Γ gap. The highest valence band is almost flat in the X-W [$\mathbf{k}=(0,1/2,0)$] direction, which makes the indirect gaps of the W point close in energy, too.

In the tetragonal phase the fundamental gap is indirect [from Z [$\mathbf{k}=(0,0,1/2)$] to Γ]. Again two other gaps (Γ-Γ and A-Γ) are close in energy. The highest valence bands along the M-Γ-Z line are nearly dispersionless and would also give rise to indirect transitions in this energy range.

In the monoclinic phase, the valence band has maxima at the two points [Γ and B [$\mathbf{k}=(1/2,0,0)$]] where the conduc-

TABLE II. Band gaps of ZrO_2 and HfO_2 (in units of eV) obtained in this work compared to previous calculations and experimental data.

	ZrO_2			HfO_2		
Method	cubic	tetra	mono	cubic	tetra	mono
			This work			
LDA	3.26	4.07	3.58	3.55	4.36	3.95
G_0W_0	4.62	5.56	4.99	4.91	5.78	5.45
GW_0	4.97	5.92	5.34	5.20	6.11	5.78
			Other theoretical work[a]			
PP-LDA	3.25	4.10	3.12			
PP-GW_0	5.55	6.40	5.42			
			Experiment			
PES+IPS		5.68,[b] 5.5[c]			5.86,[d] 5.7[c]	
EELS		5.65,[e] 5.50[f]			5.7,[g] 5.25[h]	
		5.6,[i] 5.0[j]			5.8,[j] 5.3 ± 0.5 [k]	
XPS+XAS					5.1[l]	
SE		5.8,[m] 5.25[n]			5.8,[o] 5.6,[p] 5.66–5.95[q]	

[a]Reference 4.
[b]Reference 72.
[c]Reference 73.
[d]Reference 26.
[e]Reference 74.
[f]Reference 75.
[g]Reference 28.
[h]Reference 27.
[i]Reference 76.
[j]Reference 77.
[k]Reference 78.
[l]Reference 79.
[m]Reference 19.
[n]Reference 80.
[o]Reference 22.
[p]Reference 81.
[q]Reference 23.

tion band exhibits minima. This gives four combinations of gaps that are close in energy.

The fundamental band gaps of ZrO_2 and HfO_2 in the three different phases are summarized in Table II. The band gaps from G_0W_0 are systematically smaller by about 0.3 eV than those of GW_0. In both ZrO_2 and HfO_2, the magnitude of the band gap follows the order cubic < monoclinic < tetragonal. Although the band gap itself is quite different for the different phases the GW corrections vary by less than 0.1 eV. Table II also lists theoretical band gaps for ZrO_2 from Ref. 4, in which a pseudopotential (PP) plane-wave approach was used for LDA and GW_0@LDA. While the PP-LDA band gaps for the cubic and tetragonal phase are almost identical to our all-electron (AE) results, they differ for the monoclinic phase. The PP-GW_0 corrections to the band gaps also differ from our AE calculations (the PP results are ~0.5 eV larger), which is consistent with recent findings that the PP approach has a tendency to overestimate GW band gaps as a result of core-valence partitioning and pseudoization errors.[54,82,83] In addition, a generalized plasmon pole (GPP) model was employed in Ref. 4 to treat the frequency dependence of the polarization function, whereas we applied the more accurate imaginary frequency plus analytical continuation approach in our calculations. As demonstrated in a systematic study by Flezar and Hanke for IIB-VI semiconductors,[40] the GPP approximation consistently overestimates band gaps by ~0.1 eV.

D. Comparison with experiment

Since zirconia and hafnia are traded as very promising high-κ materials, their electronic properties have been extensively studied by different experimental techniques in recent years, including visible-ultraviolet absorption or spectroscopic ellipsometry (SE),[16,19,22,23,81] electron-energy-loss spectroscopy (EELS),[27,28,74,77] x-ray photoemission spectroscopy (XPS) or ultraviolet plus IPS (Refs. 26, 72, and 73) or x-ray absorption spectroscopy.[84] Reported band gaps from these experimental studies are included in Table II. We have not attempted to group the experimental results into the three columns because samples are often thin amorphous or polycrystalline films or no structural information is provided.

The experimental band gaps for both ZrO_2 and HfO_2 are scattered between 5 and 6 eV. This is in agreement with the range we find for the different phases in our GW_0 calculations. Compared to the most recent PES+IPS experiment of Ref. 73, the band gaps from G_0W_0 are systematically underestimated by ~0.3–0.6 eV, but the GW_0 results are in much better agreement. To be more specific, the GW_0 band gap for m-ZrO_2 is still slightly underestimated by approximately 0.3 eV, but that of m-HfO_2 agrees very well. We note, however, that some caution has to be applied when comparing theoretical band gaps with experimental data. Even in techniques that probe the quasiparticle and not the optical gap, such as PES+IPS, uncertainties arise due to finite experimental res-

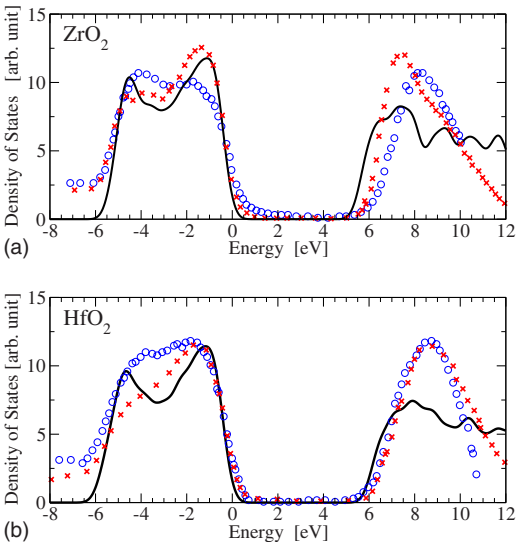

FIG. 5. (Color online) Comparison of the GW_0 DOSs (solid line) of m-ZrO_2 and m-HfO_2 with XPS+IPS data (symbols) from two different groups [circles: Bersch *et al.* (2008) (Ref. 73), crosses: Sayan *et al.* (2004) (Refs. 26 and 72)].

olution and problems in band-edge determination. Band tails from imperfections in the sample, surface adsorbants, and substrate emission can wash out the band edges[73] and the final value may depend on the chosen energy region for the fitting scheme employed to extract the band edges.[73] Other techniques, e.g., optical or x-ray absorption do not probe the fundamental gap directly and additional contributions coming from, e.g., the electron-hole interaction have to be taken into account. Last but not least approximations on the theory side (e.g., the neglect of electron-phonon coupling[60–64] or vertex corrections[40,85–87]) would have to be taken into account, too.

It is therefore illuminating to compare our calculations directly to PES+IPS spectra. Figure 5 shows the GW_0 density of states and the PES+IPS data from two different groups.[26,72,73] In both studies the samples are amorphous thin films and the electron kinetic energy (in IPS) is in the same range (18–22 eV in Refs. 26 and 72 vs 20.3 eV in Ref. 73) but the photon energies (in PES) differ (soft x rays of 120–400 eV in Refs. 26 and 72 vs 40.8 eV in Ref. 73). In general, the agreement between the GW_0 results and the experimental spectra is quite remarkable. For ZrO_2, the two experimental data sets differ quite significantly in their position of the main IPS peak, although their edges appear at almost the same energy, while the GW_0 conduction band is slightly lower in energy. For HfO_2, the two experimental spectra are nearly identical, and the agreement with the GW_0 DOS is even better than for ZrO_2. The remaining difference in the peak shape between theory and experiment could be due to final state effects that are not taken into account in the theory or the fact that the experimental samples are amorphous.

Another important quantity is the binding energy of the Hf $4f$ states, which is often used in the characterization of hafnia samples.[26,28,73,88] Since we have not included spin-orbit coupling in our *GW* calculations we will consider only the j-averaged $4f$ binding energy, $\bar{\epsilon}_{4f} \equiv \frac{4}{7}\epsilon_{4f_{7/2}} + \frac{3}{7}\epsilon_{4f_{5/2}}$ (the spin-orbit splitting obtained from LDA calculations is 1.7 eV, in good agreement with experiment). Different experimental measurements give essentially the same $4f$ level energies. The measured j-averaged $4f$ binding energy is approximately 14.5–14.9 eV with respect to the VBM. The slight variation in the experimental data sets arises mainly from uncertainties in the determination of the VB edge.[26,28,73] Our GW_0 studies give $4f$ binding energies of 14.5, 13.9, and 13.6 eV for the cubic, tetragonal, and monoclinic phases of hafnia, respectively. For the monoclinic phase, which is the most prevalent in experiment, our GW_0 $4f$ binding energy is underestimated by about 1 eV. This is a considerable improvement over the LDA underestimation of $\simeq$4.5 eV (see also Fig. 2).

E. Structural deformations

As mentioned in the previous section, experimental values for the band gaps of ZrO_2 and HfO_2 show a large variation. One of the many possible reasons is the dependence of the electronic on the atomic structure, i.e., morphology, crystal structure, and chemical composition of the sample. These factors, although often difficult to control experimentally, can be analyzed in theoretical calculations. Here we use the transformation of the cubic to the tetragonal phase as example to investigate the effects of structural changes. The two phases can be stabilized by bivalent or trivalent dopants, which may result in different equilibrium structures than those of the pure phases (that are only stable at high temperatures). The tetragonal phase of HfO_2 is of particular interest for the following reasons: (1) it can form a lattice-matched interface with silicon with a minimum number of dangling bonds and a lattice mismatch of less than 5%;[28] (2) it can be stabilized by bivalent or trivalent oxides with a *lower* doping concentration than the cubic structure, and therefore is more accessible at room temperature; and (3) it can exist in polycrystalline or amorphous thin films.

We first consider the cubic phase of ZrO_2 and HfO_2 and investigate how the volume deformation (hydrostatic strain) affects their electronic properties. The latter is usually quantified by the so-called volume deformation potential, $a_V \equiv dE_g/d\ln(V/V_0)$, where V_0 is the equilibrium volume. Deformation potentials are one of the key parameters in practical materials engineering and device design.[89] For different materials the magnitude of a_V depends strongly on the chemical bonding[89] and larger ionicity and weaker covalency typically give smaller a_V.

Figure 6 shows the LDA and GW_0 band gaps of cubic ZrO_2 and HfO_2 for different unit-cell volumes. Compared to *sp* semiconductors with pronounced covalent bonding,[89,90] the effect of the volume deformation on the band gap is relatively weak for ZrO_2 and HfO_2. Reducing or increasing the volume by as much as 5% leads to band gap changes of less than 0.2 eV. A linear fit yields the hydrostatic volume deformation potentials listed in Table III. Three facts are noteworthy: (1) the magnitude of a_V is noticeably larger for ZrO_2 than for HfO_2; (2) the difference between a_V(X-X) and a_V(X-Γ) is much larger in ZrO_2 than in HfO_2; and (3) The GW_0 corrections are more pronounced in ZrO_2. These features are consistent with the notion that HfO_2 is more ionic

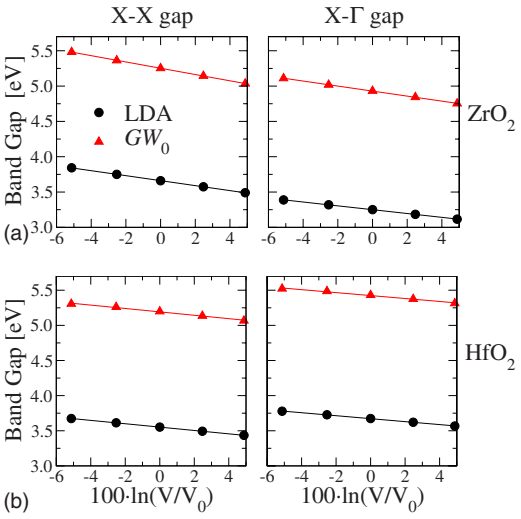

FIG. 6. (Color online) Band-gap variation in LDA and GW_0 as a function of volume for cubic ZrO_2 and HfO_2. V_0 is the experimental equilibrium volume.

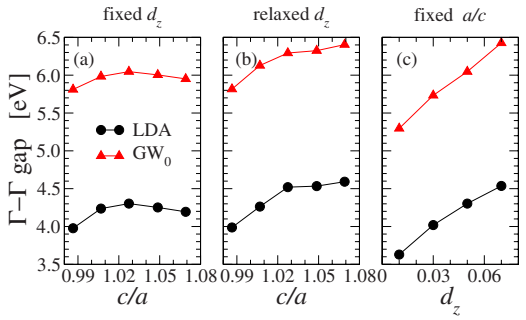

FIG. 7. (Color online) LDA and GW_0 band gaps at the Γ point in tetragonal hafnia (a) as a function of the c/a ratio with fixed d_z, (b) as a function of the c/a ratio with relaxed d_z, and (c) as a function of d_z with fixed a and c.

than ZrO_2. Wei and Zunger concluded from a systematic investigation of diamond and zinc-blende semiconductors that the deformation potential decreases as the ionicity increases.[89] Stronger covalence implies that the VBM and CBM states have stronger bonding-antibonding character, which is sensitive to the change in the bond length and varies at different **k** in the Brillouin zone.

We will now address the question why the tetragonal phase has a much larger band gap than the other two phases by investigating the effects of the cubic-to-tetragonal transformation on the electronic band structure of HfO_2. We first study the band-structure evolution for c/a deviations away from 1, i.e., that of the cubic phase. We found that even at $c/a=1$, d_z is still finite (~ 0.05) and increases linearly as c/a deviates from 1. A noticeable feature we have observed in t-HfO_2 is that while the CBM is always located at Γ[**k** $=(0,0,0)$], **k** corresponding to VBM ($\mathbf{k}_{\mathrm{VBM}}$) is very sensitive to the variation in structural parameters c/a and d_z. For example, fixing a and c to experimental values and varying d_z, $\mathbf{k}_{\mathrm{VBM}}$ changes from $(\frac{1}{2},\frac{1}{2},0)$ at $d_z=0.01$, to $(\frac{1}{2},\frac{1}{2},\frac{1}{2})$ at $d_z=0.03$, $(0,0,\frac{1}{2})$ at $d_z=0.05$, and $(\frac{1}{4},\frac{1}{4},0)$ at $d_z=0.07$. Despite the sensitivity of the VBM to variations in the structural parameters the direct gap at Γ is only slightly larger than the minimal indirect gap. We will therefore mainly focus on the direct gap at Γ.

Figure 7(a) shows the gap at Γ as a function of c/a with d_z fixed at 0.05. The band gap changes only slightly for varying c/a, and interestingly shows a maximum at $c/a \simeq 1.03$, the equilibrium c/a value. Since the equilibrium value of d_z is strongly correlated with c/a, we further study the effect of varying c/a with relaxed d_z [Fig. 7(b)]. In this case, the band gap changes much more strongly as c/a increases, in particular, when c/a is smaller than ~ 1.03. To further clarify the role of d_z, we investigate the band gap of t-HfO_2 as a function of d_z at fixed lattice constants (a and c) [Fig. 7(c)]. Increasing d_z from 0.01 to 0.07, the direct gap at Γ increases almost linearly by more than 1 eV. We can conclude from these studies that the main factor that contributes to the large band gap of t-HfO_2 is the internal distortion of the oxygen atoms.

TABLE III. Hydrostatic band-gap deformation potential (eV) of cubic ZrO_2 and HfO_2 in LDA and GW_0.

	X-X gap		X-Γ gap	
	LDA	GW_0	LDA	GW_0
ZrO_2	−3.53	−4.45	−2.71	−3.55
HfO_2	−2.39	−2.41	−2.11	−2.10

IV. CONCLUSIONS

To summarize, in this work we have employed many-body perturbation theory in the GW approach to investigate the quasiparticle band structure of crystalline ZrO_2 and HfO_2 in the cubic, tetragonal, and monoclinic phase. We found that the GW_0 approximation, with partial self-consistency in constructing G, gives band gaps of ZrO_2 and HfO_2 that are in better agreement with experiment than G_0W_0. ZrO_2 and HfO_2 have very similar electronic band structures; small differences between them can be explained by the difference in ionicity, which is already captured by the LDA. The filled f states in HfO_2 have little effect on the GW corrections. On the other hand, GW significantly increase the binding energy of the semicore f states compared to LDA, bringing them much closer to the experimental value. We observe nearly identical GW corrections for the three different phases, despite band-gap differences between them of almost 1 eV. The GW_0 density of states agrees very well with available direct and inverse photoemission spectra within the uncertainty of the experimental resolution and sample quality. With respect to structural deformations we find that the magnitude of the volume deformation potential is significantly smaller in cubic ZrO_2 and HfO_2 than in conventional sp semiconductors. For tetragonal HfO_2 a pronounced sensitivity between the relative oxygen displacement and the electronic band structures was observed that explains the larger gap of the tetragonal phase. Our work therefore indicates that the GW approach can describe the quasiparticle band structure of wide-gap oxides with empty d states and/or fully filled semicore f

states well. We note however, that the electron-hole (excitonic) and the electron-phonon interaction, which have been neglected in this study, may play a considerable role in ZrO_2 and HfO_2, as indicated by a recent study on TiO_2.[64] Further studies in this direction and more refined experiments are clearly needed for a more unambiguous comparison between experiment and theory.

ACKNOWLEDGMENTS

We acknowledge fruitful discussions with Xinzheng Li. We thank Peter Kratzer and Kazuhito Nishitani for helpful discussions in the early stage of this work. This work was in part funded by the EU's Sixth Framework Programme through the NANOQUANTA (Grant No. NMP4-CT-2004-500198) network of excellence and the EU's Seventh Framework Programme through the European Theoretical Spectroscopy Facility e-Infrastructure (Grant No. 211956). Patrick Rinke acknowledges the support of the Deutsche Forschungsgemeinschaft.

*Present address: College of Chemistry and Molecular Engineering, Peking University, Beijing, China.

[1] G. D. Wilk, R. M. Wallace, and J. M. Anthony, J. Appl. Phys. **89**, 5243 (2001).
[2] J. Robertson, Rep. Prog. Phys. **69**, 327 (2006).
[3] D. R. Clarke and C. G. Levi, Annu. Rev. Mater. Res. **33**, 383 (2003).
[4] B. Králik, E. K. Chang, and S. G. Louie, Phys. Rev. B **57**, 7027 (1998).
[5] J. Dąbrowski, V. Zavodinsky, and A. Fleszar, Microelectron. Reliab. **41**, 1093 (2001).
[6] P. W. Peacock and J. Robertson, J. Appl. Phys. **92**, 4712 (2002).
[7] L. K. Dash, N. Vast, P. Baranek, M. C. Cheynet, and L. Reining, Phys. Rev. B **70**, 245116 (2004).
[8] J. Robertson, K. Xiong, and S. J. Clark, Thin Solid Films **496**, 1 (2006).
[9] P. Broqvist and A. Pasquarello, Appl. Phys. Lett. **89**, 262904 (2006).
[10] J. L. Gavartin, D. Munoz Ramo, A. L. Shluger, G. Bersuker, and B. H. Lee, Appl. Phys. Lett. **89**, 082908 (2006).
[11] F. A. Cotton, G. Wilkinson, C. A. Murillo, and M. Bochmann, *Advanced Inorganic Chemistry* (Wiley, New York, 2000).
[12] W.-K. Li, G.-D. Zhou, and T. C. W. Mak, *Advanced Structural Inorganic Chemistry* (Oxford University Press, Oxford, 2008).
[13] M. Gutowski, J. E. Jaffe, C.-L. Liu, M. Stoker, R. I. Hedge, R. S. Rai, and P. J. Tobin, Appl. Phys. Lett. **80**, 1897 (2002).
[14] G.-M. Rignanese, J. Phys.: Condens. Matter **17**, R357 (2005).
[15] S. Stemmer, Z. Q. Chen, W. J. Chu, and T. P. Ma, J. Microsc. **210**, 74 (2003).
[16] Y. J. Cho, N. V. Nguyen, C. A. Richter, J. R. Ehrstein, B. H. Lee, and J. C. Lee, Appl. Phys. Lett. **80**, 1249 (2002).
[17] J. Aarik, H. Mändar, M. Kirm, and L. Pung, Thin Solid Films **466**, 41 (2004).
[18] T. Ito, M. Maeda, K. Nakamura, H. Kato, and Y. Ohki, J. Appl. Phys. **97**, 054104 (2005).
[19] M. Balog, M. Schieber, M. Michiman, and S. Patai, Thin Solid Films **41**, 247 (1977).
[20] S.-G. Lim, S. Kriventsov, T. N. Jackson, J. H. Haeni, D. G. Schlom, A. M. Balbashov, R. Uecker, P. Reiche, J. L. Freeouf, and G. Lucovsky, J. Appl. Phys. **91**, 4500 (2002).
[21] A. Callegari, E. Cartier, M. Gribelyuk, H. Okorn-Schmidt, and T. Zable, J. Appl. Phys. **90**, 6466 (2001).
[22] W. J. Zhu, T. Tamagawa, M. Gibson, T. Furukawa, and T. P. Ma, IEEE Electron Device Lett. **23**, 649 (2002).
[23] M. Modreanu, P. K. Hurley, B. J. O'Sullivan, B. O'Looney, J.-P. Senateur, H. Rousell, F. Rousell, M. Audier, C. Dubourdieu, I. W. Boyd Q. Fang, T. L. Leedham, S. A. Rushworth, A. C. Jones, H. O. Davies, and C. Jimenez, Proc. SPIE **4876**, 1236 (2003).
[24] N. V. Nguyen, J.-P. Han, J. Y. Kim, E. Wilcox, Y. J. Cho, W. Zhu, Z. Luo, and T. P. Ma, International Conference on Characterization and Meterology for ULSI Technology, edited by D. G. Seiler, A. C. Diebold, T. J. Shaffner, R. McDonald, S. Zollner, R. P. Khosla, and E. M. Secula (AIP Press, Melville, NY, 2003), pp. 181–185.
[25] J. Frandon, B. Brousseau, and F. Pradal, Phys. Status Solidi B **98**, 379 (1980).
[26] S. Sayan, T. Emge, E. Garfunkel, X. Zhao, L. Wielunski, R. A. Bartynski, D. Vanderbilt, J. S. Suehle, S. Suzer, and M. Banaszak-Holl, J. Appl. Phys. **96**, 7485 (2004).
[27] H. Y. Yu, M. F. Li, B. J. Cho, C. C. Yeo, M. S. Joo, D.-L. Kwong, J. S. Pan, C. H. Ang, J. Z. Zheng, and S. Ramanathan, Appl. Phys. Lett. **81**, 376 (2002).
[28] R. Puthenkovilakam and J. P. Chang, J. Appl. Phys. **96**, 2701 (2004).
[29] V. V. Afanas'ev, A. Stesmans, F. Chen, X. Shi, and S. A. Campbell, Appl. Phys. Lett. **81**, 1053 (2002).
[30] K. Xiong, J. Robertson, M. C. Gibson, and S. J. Clark, Appl. Phys. Lett. **87**, 183505 (2005).
[31] J. Robertson, Eur. Phys. J.: Appl. Phys. **28**, 265 (2004).
[32] L. Hedin and B. I. Lundqvist, Solid State Phys. **23**, 1 (1969).
[33] F. Aryasetiawan and O. Gunnarsson, Rep. Prog. Phys. **61**, 237 (1998).
[34] W. G. Aulbur, L. Jönsson, and J. W. Wilkins, Solid State Phys. **54**, 1 (2000).
[35] P. Rinke, A. Qteish, J. Neugebauer, and M. Scheffler, Phys. Status Solidi B **245**, 929 (2008).
[36] S. Kobayashi, A. Yamasaki, and T. Fujiwara, Jpn. J. Appl. Phys., Part 1 **42**, 6946 (2003).
[37] R. Shaltaf, T. Rangel, M. Grüning, X. Gonze, G.-M. Rignanese, and D. R. Hamann, Phys. Rev. B **79**, 195101 (2009).
[38] M. Rohlfing, P. Krüger, and J. Pollmann, Phys. Rev. Lett. **75**, 3489 (1995).
[39] M. Rohlfing, P. Krüger, and J. Pollmann, Phys. Rev. B **57**, 6485 (1998).
[40] A. Fleszar and W. Hanke, Phys. Rev. B **71**, 045207 (2005).
[41] F. Aryasetiawan and O. Gunnarsson, Phys. Rev. Lett. **74**, 3221 (1995).
[42] S. Massidda, A. Continenza, M. Posternak, and A. Baldereschi, Phys. Rev. B **55**, 13494 (1997).
[43] S. V. Faleev, M. van Schilfgaarde, and T. Kotani, Phys. Rev.

Lett. **93**, 126406 (2004).
[44] M. Gatti, F. Bruneval, V. Olevano, and L. Reining, Phys. Rev. Lett. **99**, 266402 (2007).
[45] A. N. Chantis, M. van Schilfgaarde, and T. Kotani, Phys. Rev. B **76**, 165126 (2007).
[46] H. Jiang, R. I. Gomez-Abal, P. Rinke, and M. Scheffler, Phys. Rev. Lett. **102**, 126403 (2009).
[47] L. Hedin, Phys. Rev. **139**, A796 (1965).
[48] M. S. Hybertsen and S. G. Louie, Phys. Rev. B **34**, 5390 (1986).
[49] R. W. Godby, M. Schlüter, and L. J. Sham, Phys. Rev. B **36**, 6497 (1987).
[50] P. Rinke, A. Qteish, J. Neugebauer, C. Freysoldt, and M. Scheffler, New J. Phys. **7**, 126 (2005).
[51] M. Shishkin and G. Kresse, Phys. Rev. B **75**, 235102 (2007).
[52] P. Blaha, K. Schwarz, G. K. H. Madsen, D. Kvasnicka, and J. Luitz, *WIEN2k, An Augmented Plane Wave Plus Local Orbitals Program for Calculating Crystal Properties*, edited by K. Schwarz (Technische Universität Wien, Austria, 2001).
[53] K. Schwarz, P. Blaha, and G. K. H. Madsen, Comput. Phys. Commun. **147**, 71 (2002).
[54] R. Gomez-Abal, X. Li, M. Scheffler, and C. Ambrosch-Draxl, Phys. Rev. Lett. **101**, 106404 (2008).
[55] R. Gomez-Abal, X. Li, H. Jiang, and M. Scheffler (unpublished).
[56] In WIEN2K DFT calculations the following parameters for the FP-(L)APW+lo basis were used: muffin-tin (MT) radii $R_{\mathrm{MT}}=2.0$ bohr for zirconium and hafnium, 1.8 bohr for oxygen; wave functions in the MT spheres were expanded in spherical harmonics with l up to $l_{\max}=10$; the potential by cubic harmonics l up to $l_{\max}=4$; the energy cutoff for interstitial plane waves was 205 eV ($R_{\mathrm{MT}}\times K_{\max}=7.0$). In the *GW* calculations, all important convergence parameters have been monitored to achieve an overall numerical accuracy of $\simeq 0.05$ eV. The Brillioun zone was sampled with $4\times4\times4$, $4\times4\times3$, and $2\times2\times2$ **k** meshes for the cubic, tetragonal, and monoclinic phase, respectively, and unoccupied states with energy up to 136 eV were taken into account.
[57] H. Jiang, R. I. Gomez-Abal, P. Rinke, and M. Scheffler (unpublished).
[58] G. M. Rignanese, X. Gonze, G. Jun, K. Cho, and A. Pasquarello, Phys. Rev. B **69**, 184301 (2004).
[59] G. M. Rignanese, X. Gonze, G. Jun, K. Cho, and A. Pasquarello, Phys. Rev. B **70**, 099903(E) (2004).
[60] R. van Leeuwen, Phys. Rev. B **69**, 115110 (2004).
[61] A. Marini, Phys. Rev. Lett. **101**, 106405 (2008).
[62] E. Kioupakis, P. Rinke, A. Schleife, F. Bechstedt, and C. G. Van de Walle (unpublished).
[63] M. Cardona, Sci. Technol. Adv. Mater. **7**, S60 (2006).
[64] P. Rinke, A. Greuling, A. Janotti, H. Jiang, E. Kioupakis, M. Rohlfing, M. Scheffler, and C. G. Van de Walle (unpublished).
[65] W. E. Pickett, H. Krakauer, and P. B. Allen, Phys. Rev. B **38**, 2721 (1988).
[66] G. H. Chen, Z. F. Hou, X. G. Gong, and Q. Li, J. Appl. Phys. **104**, 074101 (2008).
[67] S. V. Ushakov, A. Navrotsky, Y. Yang, S. Stemmer, K. Kukli, M. Ritala, M. A. Leskelä, P. Fejes, A. Demkov, C. Wang, B.-Y. Nguyen, D. Triyoso, and P. Tobin, Phys. Status Solidi B **241**, 2268 (2004).
[68] J. E. Jaffe, R. A. Bachorz, and M. Gutowski, Phys. Rev. B **72**, 144107 (2005).
[69] W. Zheng, J. K. H. Bowen, J. Li, I. Dabkowska, and M. Gutowski, J. Phys. Chem. A **109**, 11521 (2005).
[70] T. V. Perevalov, V. A. Gritsenko, S. B. Erenburg, A. M. Badalyan, H. Wong, and C. W. Kim, J. Appl. Phys. **101**, 053704 (2007).
[71] R. W. Godby, M. Schlüter, and L. J. Sham, Phys. Rev. B **37**, 10159 (1988).
[72] S. Sayan, R. A. Bartynski, X. Zhao, E. P. Gusev, D. Vanderbilt, M. Croft, M. Banaszak-Holl, and E. Garfunkel, Phys. Status Solidi B **241**, 2246 (2004).
[73] E. Bersch, S. Rangan, R. A. Bartynski, E. Garfunkel, and E. Vescovo, Phys. Rev. B **78**, 085114 (2008).
[74] R. Puthenkovilakam and J. P. Chang, Appl. Phys. Lett. **84**, 1353 (2004).
[75] S. Miyazaki, J. Vac. Sci. Technol. B **19**, 2212 (2001).
[76] H. Nohira, W. Tsai, W. Besling, E. Young, J. Petry, T. Conard, W. Vandervorst, S. De Gendt, M. Heyns, J. Maes, and M. Tuominen, J. Non-Cryst. Solids **303**, 83 (2002).
[77] N. Ikarashi and K. Manabe, J. Appl. Phys. **94**, 480 (2003).
[78] M. C. Cheynet, S. Pokrant, F. D. Tichelaar, and J.-L. Rouviere, J. Appl. Phys. **101**, 054101 (2007).
[79] S. Toyoda, J. Okabayashi, H. Kumigashira, M. Oshima, K. Ono, M. Niwa, K. Usuda, and N. Hirashita, J. Electron Spectrosc. Relat. Phenom. **137-140**, 141 (2004).
[80] L. Zhu, Q. Fang, G. He, M. Liu, X. Xu, and L. Zhang, Mater. Sci. Semicond. Process. **9**, 1025 (2006).
[81] N. V. Nguyen, S. Sayan, I. Levin, J. R. Ehrstein, I. J. R. Baumvol, C. Driemeier, C. Krug, L. Wielunski, P. Y. Hung, and A. Diebold, J. Vac. Sci. Technol. A **23**, 1706 (2005).
[82] W. Ku and A. G. Eguiluz, Phys. Rev. Lett. **89**, 126401 (2002).
[83] M. L. Tiago, S. Ismail-Beigi, and S. G. Louie, Phys. Rev. B **69**, 125212 (2004).
[84] G. Lucovsky, Y. Zhang, J. L. Whitten, D. G. Schlom, and J. L. Freeouf, Microelectron. Eng. **72**, 288 (2004).
[85] F. Bruneval, F. Sottile, V. Olevano, R. Del Sole, and L. Reining, Phys. Rev. Lett. **94**, 186402 (2005).
[86] M. Shishkin, M. Marsman, and G. Kresse, Phys. Rev. Lett. **99**, 246403 (2007).
[87] A. J. Morris, M. Stankovski, K. T. Delaney, P. Rinke, P. García-González, and R. W. Godby, Phys. Rev. B **76**, 155106 (2007).
[88] M. D. Ullrich, J. G. Hong, J. E. Rowe, G. Lucovsky, A. S.-Y. Chan, and M. T. E., J. Vac. Sci. Technol. B **21**, 1071 (2003).
[89] S.-H. Wei and A. Zunger, Phys. Rev. B **60**, 5404 (1999).
[90] P. Rinke, M. Winkelnkemper, A. Qteish, D. Bimberg, J. Neugebauer, and M. Scheffler, Phys. Rev. B **77**, 075202 (2008).